

ON THE EVOLUTION OF THE γ - AND X-RAY LUMINOSITIES OF PULSAR WIND NEBULAE

F. MATTANA,^{1,2} M. FALANGA,³ D. GÖTZ,³ R. TERRIER,¹ P. ESPOSITO,^{2,4,5}
A. PELLIZZONI,² A. DE LUCA,^{2,6,5} V. MARANDON,¹ A. GOLDWURM,^{1,3} P. A. CARAVEO²

Draft version November 15, 2018

ABSTRACT

Pulsar wind nebulae are a prominent class of very high energy ($E > 0.1$ TeV) Galactic sources. Their γ -ray spectra are interpreted as due to inverse Compton scattering of ultrarelativistic electrons on the ambient photons, whereas the X-ray spectra are due to synchrotron emission. We investigate the relation between the γ - and X-ray emission and the pulsars' spin-down luminosity and characteristic age. We find that the distance-independent γ - to X-ray flux ratio of the nebulae is inversely proportional to the spin-down luminosity, ($\propto \dot{E}^{-1.9}$), while it appears proportional to the characteristic age, ($\propto \tau_c^{2.2}$), of the parent pulsar. We interpret these results as due to the evolution of the electron energy distribution and the nebular dynamics, supporting the idea of so-called relic pulsar wind nebulae. These empirical relations provide a new tool to classify unidentified diffuse γ -ray sources and to estimate the spin-down luminosity and characteristic age of rotation powered pulsars with no detected pulsation from the X- and γ -ray properties of the associated pulsar wind nebulae. We apply these relations to predict the spin-down luminosity and characteristic age of four (so far unpulsing) candidate pulsars associated to wind nebulae.

Subject headings: pulsars : general — radiation mechanisms: non-thermal — supernova remnants — X-rays : stars — gamma rays: observations

1. INTRODUCTION

Pulsar Wind Nebulae (PWNe) arise when the wind ejected from a rotation powered pulsar is confined by the pressure of the surrounding medium, be it their supernova remnant or compressed interstellar gas (see Gaensler & Slane 2006, for a review). The Galactic survey performed by the *H.E.S.S.* experiment (*High Energy Stereoscopic System*, Hinton 2004) has detected several PWNe making them a prominent class of Very High Energy Galactic sources (Aharonian et al. 2006e; Gallant 2007; Funk 2007). In addition to the classical investigations through radio and X-ray astronomies, Very High Energy γ -rays (VHE γ -rays, $E > 0.1$ TeV) provide a new probe of the physical conditions in PWNe (e.g., de Jager & Djannati-Atai 2008).

The PWN broad-band radiation is most likely due to electron-positron pairs of the pulsar wind generated close to the magnetosphere. The wind flow is ultrarelativistic (bulk Lorentz factor $\Gamma_W \sim 10^6$ in the Crab Nebula; Kennel & Coroniti 1984a,b), until it experiences a strong shock, where electrons are accelerated. After the shock, the flow speed is sub-relativistic at the outer edge of the PWN. Depending on the radiation mechanisms at work, the electrons can produce photons in different energy ranges: while synchrotron radiation yields pho-

tons with energies up to several MeV, inverse Compton scattering of the ambient photon field can produce high energy photons, up to tens of TeV.

The electrons responsible for the PWN γ -ray emission (here after γ -ray electrons) are likely less energetic than those generating the X-ray one (X-ray electrons), their synchrotron radiation lying at infrared, optical, or ultraviolet frequencies. For typical nebular magnetic field intensities ($B \sim 1\text{--}100 \mu\text{G}$), synchrotron photons with energy ~ 1 keV are produced by electrons with Lorentz factor $\sim 0.3\text{--}3 \times 10^8$. The Cosmic Background Radiation, the dust-scattered light, and the starlight provide the target photons for inverse Compton scattering, with typical photon energies around 10^{-3} eV, 10^{-2} eV, and 1 eV, respectively. In the Thomson regime, photons with energy ~ 1 TeV are produced by electrons with Lorentz factor $\sim 0.1\text{--}3 \times 10^7$. Due to their different energies, the cooling time of the X-ray electrons is smaller than the one of the γ -ray electrons. Therefore, the X-ray emission traces the recent history of the nebula, whereas the γ -ray emission traces a longer history, possibly up to the pulsar birth. The different lifetime of the electrons, together with the interaction with the ambient medium, can lead to the significant projected angular separation, sometimes measured between the peaks of the γ - and X-ray brightness profiles (e.g. G18.0-0.7, Aharonian et al. 2006d). Since the source of injected electrons, the pulsar rotational energy loss rate dubbed spin-down luminosity, decreases as time goes by, we expect a different evolution of the γ - and X-ray luminosities, following the particle aging and the pulsar spin-down.

In this paper we address first the correlations between the PWN VHE γ -ray luminosities (1–30 TeV) and their X-ray luminosities (2–10 keV) with the spin-down luminosities, \dot{E} , and the characteristic ages, τ_c , of their pulsars. Next we consider the behaviour of the ratio be-

¹ AstroParticule et Cosmologie (APC), CNRS, Université Paris 7 Denis Diderot, F-75205 Paris, France; fabio.mattana@apc.univ-paris7.fr.

² INAF –Istituto di Astrofisica Spaziale e Fisica Cosmica, via Bassini 15, I-20133 Milano, Italy

³ CEA Saclay, DSM/IRFU/Service d'Astrophysique, F-91191 Gif-sur-Yvette, France

⁴ Università degli Studi di Pavia, Dipartimento di Fisica Nucleare e Teorica, via Bassi 6, I-27100 Pavia, Italy

⁵ Istituto Nazionale di Fisica Nucleare, sezione di Pavia, via Bassi 6, I-27100 Pavia, Italy

⁶ Istituto Universitario di Studi Superiori, v.le Lungo Ticino Sforza 56, I-27100 Pavia, Italy

tween the gamma and X-ray luminosity as a function of the pulsar spin-down power and age. These relations are discussed in the frame of an evolving electron energy population.

2. OBSERVED CORRELATIONS

In Table 1 we report a sample of the identified PWNe observed by the *H.E.S.S.* experiment. We further included six candidate PWNe, selecting unidentified *H.E.S.S.* diffuse sources located near young and energetic pulsars, with $\tau_c \lesssim 100$ kyr and $\dot{E} > 10^{35}$ erg s $^{-1}$. These parameters are defined as $\dot{E} \equiv 4\pi^2 I \dot{P} / P^3$ and $\tau_c \equiv P / 2\dot{P}$, where P is the pulsar spin period, \dot{P} its derivative, and $I \equiv 10^{45}$ gm cm 2 the moment of inertia. We calculated \dot{E} and τ_c using the P and \dot{P} values reported in the Australia Telescope National Facility (ATNF) pulsar catalogue⁷ (Manchester et al. 2005). The γ -ray fluxes, F_γ , are derived from literature and computed in the 1–30 TeV energy band, with statistical errors estimated with standard Montecarlo propagation technique. The lower energy value corresponds to the highest observed detection threshold. The upper value of 30 TeV reduces the bias of possible unmeasured high-energy cut-offs. The unabsorbed X-ray fluxes, F_X , have been derived from literature based on X-ray imaging observatories, and converted in the 2–10 keV energy band. The lower energy is chosen in order to minimize the contamination by possible thermal components due to the pulsar or supernova remnant. When it was possible to single out the PWN from the pulsar component, only the PWN flux is reported.

We investigated the relations between the different luminosities and the pulsar parameters, using the data collected in Table 1. The γ -ray luminosities, L_γ , do not appear correlated with the pulsar spin-down luminosities \dot{E} , nor they do with the characteristic ages τ_c , as shown in Fig. 1 (top panels). This is at variance with the observed PWNe X-ray luminosities, for which a scaling relation is apparent with both \dot{E} and τ_c (Fig. 1, middle panels). The weighted least square fit on the whole dataset yields

$$\log_{10} L_X = (33.8 \pm 0.04) + (1.87 \pm 0.04) \log_{10} \dot{E}_{37}. \quad (1)$$

All the uncertainties are at 1σ level, and $\dot{E} = \dot{E}_{37} \times 10^{37}$ erg s $^{-1}$. The $L_X - \dot{E}$ scaling is known for the pulsars as well as for the PWNe. This scaling was firstly noted by Seward & Wang (1988); further, Becker & Trümper (1997) investigate a sample of 27 pulsars with *ROSAT*, yielding the simple scaling $L_{X(0.1-2.4\text{keV})} \simeq 10^{-3} \dot{E}$. A re-analysis was performed by Possenti et al. (2002), who studied a sample of 39 pulsars observed by several X-ray observatories, accounting for the statistical and systematic errors. They found $\log_{10} L_X = (-14.36 \pm 0.01) + (1.34 \pm 0.03) \log_{10} \dot{E}$, a relation harder than Eq. (1). However, they could not separate the PWN from the pulsar contribution. A better comparison can be done with the results from Kargaltsev & Pavlov (2008), who recently used high-resolution *Chandra* data in order to decouple the PWN and the pulsar fluxes. Indeed, taking \dot{E} , τ_c , and L_{PWN}

in the 0.5–8 keV energy band⁸ from their Tables 1 and 2, we obtained as fitted values $\log_{10} L_{X(0.5-8\text{keV})} = (34.02 \pm 0.05) + (1.46 \pm 0.04) \log_{10} \dot{E}_{37}$ for their whole sample, and $\log_{10} L_{X(0.5-8\text{keV})} = (34.26 \pm 0.03) + (1.87 \pm 0.01) \log_{10} \dot{E}_{37}$ restricting the fit only to the sources also present in our sample. The latter is compatible in the terms of slope with Eq. (1), and the slight difference in normalization can be due to the different energy band.

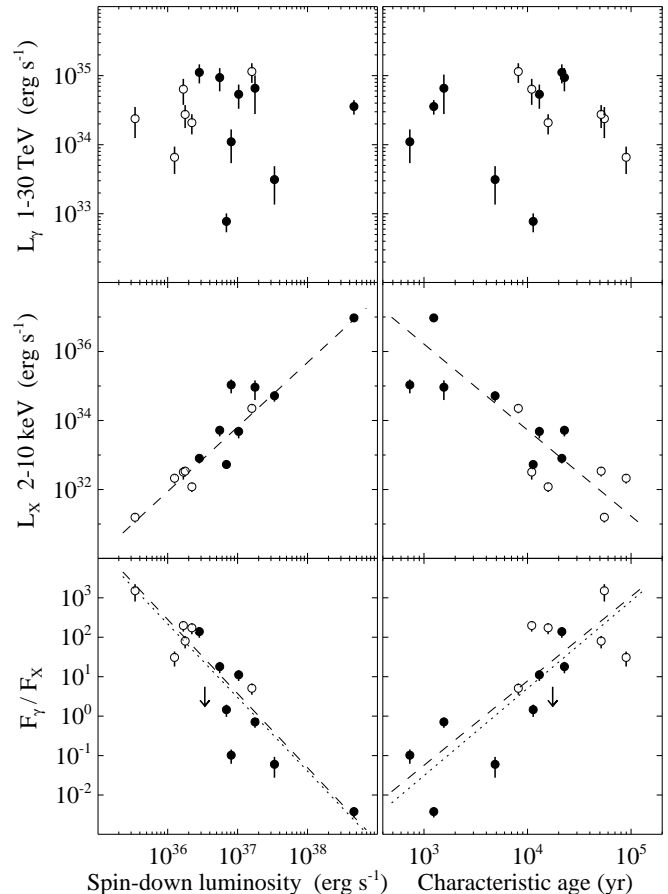


FIG. 1. — γ -ray luminosity, X-ray luminosity, and γ - to X-ray flux ratio versus pulsar spin-down luminosity, \dot{E} (left column), and characteristic age, τ_c (right column). Filled and open circles stand for identified and candidate PWNe, respectively. The upper-limit for the flux ratio of PSR B1706-44 (Aharonian et al. 2005a; Romani et al. 2005) is reported with an arrow. Also shown are the best-fit curves for identified PWNe (dotted lines), and for the whole sample (dashed lines).

X-ray sources of our whole dataset also show a dependence of L_X on τ_c , with a best-fit relation

$$\log_{10} L_X = (33.7 \pm 0.04) - (2.49 \pm 0.06) \log_{10} \tau_4, \quad (2)$$

where τ_c is in units of years. The $L_X - \tau_c$ scaling was already noted by Becker & Trümper (1997) and Possenti et al. (2002). Also in this case we compared our fit to the one derived using the whole Kargaltsev & Pavlov (2008) dataset, which results in $\log_{10} L_{X(0.5-8\text{keV})} = (34.29 \pm 0.01) - (2.03 \pm 0.01) \log_{10} \tau_4$ for their whole sample, and $\log_{10} L_{X(0.5-8\text{keV})} = (34.23 \pm$

⁸ The X-ray luminosity reported in Kargaltsev & Pavlov (2008) for Kes 75 was corrected according to the distance measured by Leahy & Tian (2008).

⁷ <http://www.atnf.csiro.au/research/pulsar/psrcat>

TABLE 1
 PROPERTIES OF WIND NEBULAE OBSERVED WITH *H.E.S.S.* AND ASSOCIATED PULSARS

Source Name	Associated Pulsar	F_γ^a (1–30 TeV) 10^{-12} erg cm $^{-2}$ s $^{-1}$	F_X^b (2–10 keV) erg cm $^{-2}$ s $^{-1}$	τ_c kyr	\dot{E} erg s $^{-1}$	Distance kpc	References
Crab	PSR B0531+21	80 (4) (16)	2.10×10^{-8}	1.2	4.6×10^{38}	$1.93^{+0.11}_{-0.11}$	1,2,3
Vela	PSR B0833–45	79 (15) (16)	5.39×10^{-11}	11	6.9×10^{36}	$0.287^{+0.019}_{-0.017}$	4,5,6
K3 in Kookaburra	PSR J1420–6048	14.5 (1.6) (2.9)	1.3×10^{-12}	13	1.0×10^{37}	$5.6^{+0.9}_{-0.8}$	7,8,9
MSH 15–52	PSR B1509–58	20.3 (1.1) (4.1)	2.86×10^{-11}	1.6	1.8×10^{37}	$5.2^{+1.4}_{-1.4}$	10,11,12
G18.0–0.7	PSR B1823–13	61 (7) (12)	4.4×10^{-13}	21	2.8×10^{36}	$3.9^{+0.4}_{-0.4}$	13,14,9
G21.5–0.9	PSR J1833–1034	2.4 (1.1) (0.5)	4.0×10^{-11}	4.9	3.4×10^{37}	$3.3^{+0.4}_{-0.5}$	15,16,9
AX J1838.0–0655	PSR J1838–0655	18.0 (2.7) (3.6)	1.0×10^{-12}	23	5.5×10^{36}	$6.6^{+0.9}_{-0.9}$	17,18,19
Kes 75	PSR J1846–0258	2.3 (0.6) (0.5)	2.27×10^{-11}	0.73	8.1×10^{36}	$6.3^{+1.2}_{-1.2}$	15,20,21
HESS J1303–631 \dagger	PSR J1301–6305	12 (1.2) (2.4)	6.2×10^{-14}	11	1.7×10^{36}	$6.6^{+1.2}_{-1.1}$	22,23,9
HESS J1616–508 \dagger	PSR J1617–5055	21 (3) (4)	4.2×10^{-12}	8.1	1.6×10^{37}	$6.7^{+0.7}_{-0.7}$	17,24,9
HESS J1702–420 \dagger	PSR J1702–4128	9.1 (3.4) (1.8)	6.0×10^{-15}	55	3.4×10^{35}	$4.7^{+0.5}_{-0.5}$	17,25,9
HESS J1718–385 \dagger	PSR J1718–3825	4.3 (1.3) (0.9)	1.4×10^{-13}	90	1.3×10^{36}	$3.6^{+0.4}_{-0.4}$	26,27,9
HESS J1804–216 \dagger	PSR B1800–21	11.8 (1.6) (2.4)	6.8×10^{-14}	16	2.2×10^{36}	$3.8^{+0.4}_{-0.5}$	17,28,9
HESS J1809–193 \dagger	PSR J1809–1917	19 (4) (4)	2.3×10^{-13}	51	1.8×10^{36}	$3.5^{+0.4}_{-0.5}$	26,29,9

\dagger Candidate sources. ^a γ -ray fluxes, statistical, and systematical errors. When not stated in the original papers, the systematic errors were assumed at the typical value of 20% as in Aharonian et al. (2006e). ^bErrors are conservatively estimated at 20%.

References.– (1) Aharonian et al. 2006c; (2) Willingale et al. 2001; (3) Trimble, V. 1973; (4) Aharonian et al. 2006a; (5) Manzali et al. 2007; (6) Dodson et al. 2003; (7) Aharonian et al. 2006b; (8) Ng et al. 2005; (9) Manchester et al. 2005; (10) Aharonian et al. 2005c; (11) Gaensler et al. 2002; (12) Gaensler et al. 1999; (13) Aharonian et al. 2006d; (14) Gaensler et al. 2003; (15) Djannati-Ataï et al. 2007; (16) Slane et al. 2000; (17) Aharonian et al. 2006e; (18) Gotthelf & Halpern 2008; (19) Davies et al. 2008 (20) Helfand et al. 2003; (21) Leahy & Tian 2008; (22) Aharonian et al. 2005d; (23) XMM public data archive; (24) Kargaltsev et al. 2008; (25) Chang et al. 2008; (26) Aharonian et al. 2007; (27) Hinton et al. 2007; (28) Kargaltsev et al. 2007; (29) Kargaltsev & Pavlov 2007.

0.02) – (2.60 \pm 0.02) $\log_{10} \tau_4$ restricting the fit only to the sources also present in our sample.

The lower panels of Fig. 1 refer to the γ - to X-ray flux ratio F_γ/F_X . There is a clear anticorrelation between F_γ/F_X and \dot{E} , spanning over four decades in \dot{E} and seven decades in F_γ/F_X (Fig. 1, bottom left panel). Considering only the identified PWNe, the correlation coefficient is $r = -0.7 \pm 0.2$; including also the candidate sources, the anticorrelation is more significant, with $r = -0.84 \pm 0.09$. The best-fit including only the identified sources yields

$$\log_{10} F_\gamma/F_X = (0.47 \pm 0.05) - (1.87 \pm 0.07) \log_{10} \dot{E}_{37}. \quad (3)$$

For all the data points, it results

$$\log_{10} F_\gamma/F_X = (0.57 \pm 0.04) - (1.88 \pm 0.05) \log_{10} \dot{E}_{37}, \quad (4)$$

compatible within the errors with the relation obtained using only the identified sources.

The γ - to X-ray flux ratio is also found to correlate with the characteristic age τ_c (Fig. 1, bottom right panel), with a correlation coefficient $r = 0.7 \pm 0.2$ for identified PWNe only, and $r = 0.75 \pm 0.13$ for the whole sample. The ordinary weighted least square fit only for the identified PWNe yields

$$\log_{10} F_\gamma/F_X = (0.70 \pm 0.06) + (2.21 \pm 0.09) \log_{10} \tau_4, \quad (5)$$

and for all the data points

$$\log_{10} F_\gamma/F_X = (0.89 \pm 0.04) + (2.14 \pm 0.07) \log_{10} \tau_4. \quad (6)$$

One should note that these correlations are based on 8 identified sources, and are consistent when the 6 candidate sources are considered. More γ -ray detections may improve their significance.

3. DISCUSSION

We found the γ - to X- ray luminosity ratio $L_\gamma/L_X = F_\gamma/F_X$ to be anticorrelated with the spin-down luminosity \dot{E} and correlated with the characteristic age τ_c . Formally, such dependencies are driven by the scaling law of the X-ray luminosity L_X , which increases with \dot{E} and decreases with τ_c , since the values of L_γ were found uncorrelated with the pulsar parameters. However, the F_γ/F_X is a distant-independent indicator which relates two electron populations, differing by energy and age. An evolution in the PWN broad-band spectrum is pointed out by Eq. (5), which implies $L_\gamma > L_X$ after ~ 5 kyr from pulsar birth. Therefore, the γ -ray emission remains efficient around $L_\gamma \sim 10^{33}$ – 10^{35} erg s $^{-1}$, while the X-ray luminosity decreases by a factor $\sim 10^6$ in 10^5 yr following the pulsar spin-down.

Such a broad-band spectral evolution can be expected on the basis of the PWNe leptonic model (Kennel & Coroniti 1984b; Chevalier 2000). In a PWN, the source of the injected electrons is the pulsar spin-down luminosity, \dot{E} . The total injection rate of the electrons can be written:

$$\dot{N} = \frac{\dot{E}}{\Gamma_W m_e c^2 (1 + \sigma)}, \quad (7)$$

where the magnetization parameter σ sets the fraction of the spin-down luminosity converted in kinetic energy of the wind. The whole spin-down luminosity is converted in particle kinetic energy for $\sigma \ll 1$, as for the Crab Nebula (Kennel & Coroniti 1984a,b). For sake of simplicity, we assume a constant wind Lorentz factor Γ_W upstream the shock. \dot{E} decreases in time as (e.g., Pacini & Salvati 1973)

$$\dot{E}(t) = \frac{\dot{E}_0}{(1 + t/t_{dec})^\beta}, \quad (8)$$

where $\dot{E}_0 \sim 10^{38}$ – 10^{40} erg s $^{-1}$ is the spin-down luminos-

TABLE 2
PWNe HOSTING A NEUTRON STAR WITHOUT DETECTED PULSATIONS

Source Name	F_γ (1–30 TeV) erg cm ⁻² s ⁻¹	F_X (2–10 keV) erg cm ⁻² s ⁻¹	τ_c^* kyr	\dot{E}^* erg s ⁻¹
G313.+0.1 Rabbit	1.0×10^{-11}	7.3×10^{-12}	~ 6	$\sim 1.5 \times 10^{37}$
G0.9+0.1	3.3×10^{-12}	5.8×10^{-12}	~ 4	$\sim 2 \times 10^{37}$
G12.8-0.0 [†]	1.3×10^{-11}	9.2×10^{-12}	~ 6	$\sim 1.5 \times 10^{37}$
HESS J1640–465 [†]	9.3×10^{-12}	1.0×10^{-12}	~ 13	$\sim 5 \times 10^{36}$

[†]Candidate sources. *Predicted values. References.— HESS J1418/G313.+0.1 Rabbit: Aharonian et al. (2006b), Ng et al. (2005); HESS J1747–281/G0.9+0.1: Aharonian et al. (2005b), Porquet et al. (2003); HESS J1813–178/G12.8–0.0: Aharonian et al. (2006e), Helfand et al. (2007); HESS J1640–465/G338.3–0.0: Aharonian et al. (2006e), Funk et al. (2007).

ity at the pulsar birth, $t_{dec} \sim 100$ – 1000 yr is a characteristic decay time, t is the time elapsed since pulsar birth ($t_0 = 0$), and $\beta = (n+1)/(n-1)$, where n is the braking index. In the following, we assume a pure dipolar magnetic field torque, i.e. $n = 3$. As the braking indices inferred from the measurement of the period and its derivatives are significantly smaller than 3 (Livingstone et al. 2007), we dealt with a generic n (see App. A), and found that the results derived from Eq. (8) are unaffected by the choice of n .

Since it depends on \dot{E} , also the particle injection rate \dot{N} decreases in time. Therefore, the total number of particles

$$N \propto \int_0^t \dot{E}(t') dt' = \dot{E}_0 t_{dec} \left(\frac{t}{t+t_{dec}} \right), \quad (9)$$

reaches a constant value $N \propto \dot{E}_0 t_{dec}$ for $t \gg t_{dec}$, and the particle supply by the pulsar becomes negligible.

The electron energy distribution $n(E, t)$ accounting for particle injection and radiative losses evolves according to the kinetic equation (e.g., Ginzburg & Syrovatskii 1964; Blumenthal & Gould 1970):

$$\frac{\partial n}{\partial t} = \frac{\partial}{\partial E} (nP) + Q, \quad (10)$$

where $Q = Q(E, t)$ is the particle distribution injected per unit time, and $P = P(E, t)$ is the radiated power per particle with energy E . The normalization of $n(E, t)$ is set by N via the injection rate: $\dot{N}(t) = \int Q(E, t) dE$.

At energies for which the radiative losses are negligible, the number of particles $n(E, t)$ with energy E at time t has the same profile of the injected distribution $Q(E)$ with a normalization set by N . Therefore,

$$n_u(E, t) \propto \int_0^t \dot{E}(t') dt' = \dot{E}_0 t_{dec} \left(\frac{t}{t+t_{dec}} \right), \quad (11)$$

where u stands for *uncooled*. As in Eq. (9), a constant value $n_u(E, t) \propto \dot{E}_0 t_{dec}$ is reached for $t \gg t_{dec}$.

The effect of the radiative losses is to limit the accumulation of particles at a given energy. After an energy-dependent cooling time $t_c(E)$, the particles with initial energy E have radiated a significant fraction of their energy (Chevalier 2000). Accounting for pitch-angle averaged synchrotron and inverse Compton in the Thomson regime energy losses, the cooling time can be written as

$$t_c(E) = \frac{9 m_e^3 c^5}{4 (1 + \xi) e^4 \gamma_E B^2} \simeq 24.5 (1 + \xi)^{-1} \gamma_7^{-1} B_5^{-2} \text{ kyr}, \quad (12)$$

where $\gamma_E = E/(m_e c^2)$ is the particle Lorentz factor, and $\xi = U_{ph}/U_B$, with U_{ph} and U_B the photon field and magnetic field energy densities, respectively ($\gamma_E = \gamma_7 \times 10^7$, $B = B_5 \times 10^{-5}$ G). When the photon field is provided by the Cosmic Background Radiation ($U_{ph} = 0.26$ eV cm⁻³), the synchrotron radiation is the main cooling process ($\xi < 1$) if $B > 3$ μ G. This condition is generally fulfilled in PWNe as the equipartition magnetic field intensity ranges in $B \sim 1$ – 100 μ G.⁹ Eq. (12) shows that the cooling time of γ -ray radiating particles, $t_{c\gamma}$, is one order of magnitude longer than that of the X-ray radiating particles, t_{cX} , e.g., for $B = 10$ μ G, $t_{c\gamma} \sim 8$ – 250 kyr, and $t_{cX} \sim 0.8$ – 8 kyr. By comparing $t_{c\gamma}$ and t_{cX} with the average characteristic ages of pulsars in TeV PWNe, the γ -radiation is produced by long-lived electrons tracing the time-integrated evolution of the nebula, even up to the pulsar birth, whereas the X-ray emission is generated by younger electrons, injected in the last thousands of years.

Only the particles injected since the last $t_c(E)$ years will contribute to $n(E, t)$. Eq. (11) is accordingly modified:

$$n_c(E, t) \propto \int_{t-t_c}^t \dot{E}(t') dt' = \frac{\dot{E}_0 t_{dec}^2 t_c}{(t-t_c+t_{dec})(t+t_{dec})}, \quad (13)$$

where c stands for *cooled*. This implies $n_c(E, t) \propto \dot{E}_0 t_{dec}^2 t_c t^{-2}$ for $t \gg \max(t_c, t_{dec})$, and hence $n_c(E, t) \propto \dot{E} t_c$ using Eq. (8).

4. CONCLUSIONS

Eqs. (11) and (13) describe the time evolution of a particle populations in two regimes, uncooled and cooled. Such an evolution is exemplified in Fig. 2 for the populations of particles producing γ -rays, n_γ , and X-rays, n_X . After the initial rise, both the particle populations reach a plateau ($t > t_{dec}$). The decrease begins when the evolution time is greater than the cooling time. As in general $t_{cX} < t_{c\gamma}$, the X-ray emission fades long before the γ -ray one.

As the characteristic ages of the pulsars powering a VHE γ -ray PWN are in the range 1–20 kyr, likely $t_{cX} < \tau_c < t_{c\gamma}$. Accordingly, the population of the X-ray electrons, n_X , is likely to be in the cooling regime, i.e., it decreases. The scaling laws $n_X \propto \tau_c^{-2}$ and $n_X \propto \dot{E}$ of Eq. (13) support the trend observed in the data, see

⁹ In radiation-dominated environment, like the Galactic Center, the inverse Compton can contribute to the cooling. In this case, the Klein-Nishina regime should be taken into account (Manolakou et al. 2007).

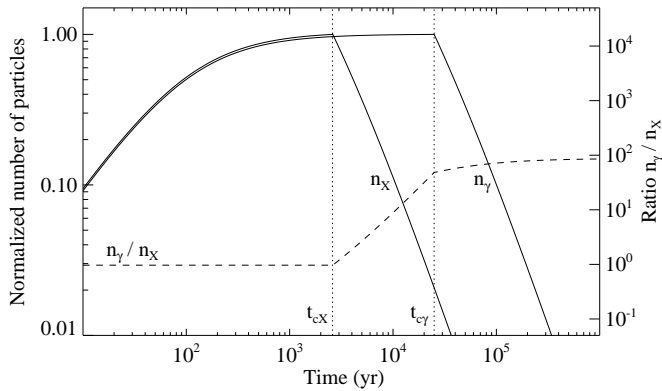


FIG. 2.— Time evolution of the number of particles radiating in VHE γ -rays, n_γ , and in X-rays, n_X (solid lines), and of their ratio (dashed line). Pulsar birth is at $t = 0$. Initial conditions for the pulsar spin-down luminosity are $\dot{E}_0 = 10^{39}$ erg s $^{-1}$ and $t_{dec} = 100$ yr. Both curves are normalized to their maximum value. After the initial rise, both particle populations reach a plateau. The fall begins at t greater than the cooling time, which is assumed to be: $t_{cX} = 2.6$ kyr for X-rays, $t_{c\gamma} = 25$ kyr for γ -rays (for a magnetic field intensity $B = 10 \mu\text{G}$, and a Lorentz factor of γ -ray radiating electrons $\gamma = 10^7$).

Eq. (1). At variance, the population of the γ -ray electrons, n_γ , is in the uncooled regime, the asymptotic limit of Eq. (11); this explains the lack of correlation between γ -ray luminosity L_γ and \dot{E} . Finally, Eqs. (11) and (13) for $t_{cX} < \tau_c < t_{c\gamma}$ imply a ratio $n_\gamma/n_X \propto t^2 \propto \dot{E}^{-1}$. Since the luminosities are roughly proportional to the population of radiating particles, finally one gets

$$L_\gamma/L_X \propto t^2 \propto \dot{E}^{-1},$$

to compare with the best-fit empirical relations $L_\gamma/L_X \propto \tau_c^{2.2}$ and $L_\gamma/L_X \propto \dot{E}^{-1.9}$, see Eqs. (5) and (3). Though the outlined model does not correctly predict the slopes, not surprisingly in being simplified, it highlights the concurrent roles of the evolving pulsar injection and of the radiative losses in producing the observed trends.

The scattering around the relations for F_γ/F_X reflects the lack of correlation between L_γ and \dot{E} . Environmental factors can affect the γ -ray luminosities, like the local energy density of the ambient photon field, or the interaction with the surrounding medium causing an enhancement in the magnetic field. Also, unmeasured pulsar properties such as the magnetic field, its orientation with respect to the spin axis, and the initial spin period might affect the pulsar wind properties.

We stress that the relations presented here are derived under several assumptions, the most important of which being that X-ray and γ -ray emitting particles are in different cooling regimes, cooled for X-rays and uncooled for γ -rays. However, the Lorentz factors ranges of the two populations get closer, and they can even overlap, if the nebular magnetic field is very high, on the order of $B=170 \mu\text{G}$. On the other hand, in the case of a young nebula with a very low magnetic field, the X-ray electrons may not have reached the cooling regime, leaving the γ -ray production to the low-energy freshly injected

electrons. Hence, PWNe with a very weak magnetic field, like 3C 58 (Slane et al. 2008), or possibly with a unusually strong one, as reported lately by Arzoumanian et al. (2008) for DA 495, could represent outliers to our derived relations. These regimes can be properly taken into account through numerical modelling of the kinetic equation (Eq. [10]). Another important assumption is a uniform and constant magnetic field: indeed high resolution imaging observations of several PWNe show a dynamical and structured nebular morphology (Gaensler & Slane 2006). The evolution of the average magnetic field is complicated by the interaction with the supernova ejecta, which is expected to occur after a few thousands of years since pulsar birth, causing global oscillations of the magnetic field intensity (e.g., Bucciantini et al. 2003). One should note that the cooling time is not well defined if it is comparable to or longer than the time scale of variation of the magnetic field. The cases of patchy or evolving magnetic field are further sources of scattering around our relations.

Given the limitations discussed above, the empirical relations in Eqs. (3) and (5) provide a new tool to estimate the spin-down luminosity and characteristic age of a pulsar lacking detected pulsation from the γ - and X-ray properties of the associated PWN. For the four candidate pulsars in Table 2, we used F_γ/F_X to predict \dot{E} and τ_c . Taking into account the average scattering (average absolute ratio) around the best fit relations, Eqs. (3) and (5), one should expect an uncertainty of a factor ~ 2.5 for \dot{E} and ~ 2.3 for τ_c considering only the eight identified sources. On the other hand, considering Eqs. (4) and (6), and including also the candidate sources, the uncertainties are ~ 2.2 for \dot{E} and ~ 2.6 for τ_c .

The correlations for F_γ/F_X hold also after including the candidate sources. The pulsars possibly associated to the candidate sources are mostly older Vela-like pulsars, with $8 \times 10^3 \text{ yr} < \tau_c < 9 \times 10^4 \text{ yr}$, and $3.4 \times 10^{35} \text{ erg s}^{-1} < \dot{E} < 1.6 \times 10^{37} \text{ erg s}^{-1}$. Due to the pulsar ages, the electrons had the time to be advected far from the pulsar, producing the offset between the γ -ray emission centroid and the pulsar position, the process leading to the so-called relic PWNe (de Jager & Djannati-Ataï 2008). The fact that all the confirmed associations contain younger pulsars is hence not surprising, as the positional coincidence is one of the main identification criteria. If the identification of candidate sources with relic PWNe is confirmed, the γ -ray luminosity would persist up to 10^5 yr, with remarkable time-integrated energy channeled in radiation ($\sim 3 \times 10^{45} - 3 \times 10^{47}$ erg).

FM, MF, and DG acknowledge the French Space Agency (CNES) for financial support. FM is also grateful for support from the Moscow St. NGO. We wish to thank the referee, P. Slane, for his very constructive comments and suggestions that helped to improve the manuscript.

APPENDIX

PARTICLE POPULATION INJECTED BY A PULSAR WITH GENERIC BRAKING INDEX

By adopting Eq. (8) for a generic braking index $n > 1$, Eqs. (11) and (13) are so modified:

$$n_u(E, t) \propto \int_0^t \dot{E}(t') dt' = \frac{\dot{E}_0 t_{dec}}{\beta - 1} \left[1 - \left(\frac{t_{dec}}{t + t_{dec}} \right)^{\beta - 1} \right], \quad (\text{A1})$$

and

$$n_c(E, t) \propto \int_{t-t_c}^t \dot{E}(t') dt' = \frac{\dot{E}_0 t_{dec}^\beta}{\beta - 1} (t_{dec} + t)^{1-\beta} \left[\left(1 - \frac{t_c}{t_{dec} + t} \right)^{1-\beta} - 1 \right]. \quad (\text{A2})$$

For $t \gg t_{dec}$ Eq. (A1) yields $n_u \propto \dot{E}_0 t_{dec}/(\beta - 1)$, while for $t \gg \max(t_c, t_{dec})$ Eq. (A2) yields $n_c \propto \dot{E}(t) t_c$. As in the case of the dipolar magnetic braking, in the uncooled regime most of the radiating particles has been injected in the early phases, whereas in the cooled regime the particle population is limited by the cooling time and follows more closely the current spin-down rate.

REFERENCES

- Aharonian, F., et al. (HESS Collaboration) 2005a, *A&A*, 432, L9
 Aharonian, F., et al. (HESS Collaboration) 2005b, *A&A*, 432, L25
 Aharonian, F., et al. (HESS Collaboration) 2005c, *A&A*, 435, L17
 Aharonian, F., et al. (HESS Collaboration) 2005d, *A&A*, 439, 1013
 Aharonian, F., et al. (HESS Collaboration) 2006a, *A&A*, 448, L43
 Aharonian, F., et al. (HESS Collaboration) 2006b, *A&A*, 456, 245
 Aharonian, F., et al. (HESS Collaboration) 2006c, *A&A*, 457, 899
 Aharonian, F., et al. (HESS Collaboration) 2006d, *A&A*, 460, 365
 Aharonian, F., et al. (HESS Collaboration) 2006e, *ApJ*, 636, 777
 Aharonian, F., et al. (HESS Collaboration) 2007, *A&A*, 472, 489
 Aharonian, F., et al. (HESS Collaboration) 2008, *A&A*, 484, 435
 Arzoumanian, Z., Safi-Harb, S., Landecker, T. L., Kothes, R., & Camilo, F. 2008, *ApJ*, in press (astro-ph/0806.3766)
 Becker, W., & Trümper, J. 1997, *A&A*, 326, 682
 Bucciantini, N., Blondin, J. M., Del Zanna, L., & Amato, E. 2003, *A&A*, 405, 617
 Blumenthal, G. R. & Gould, R. J. 1970, *Rev. Mod. Phys.*, 42, 237
 Chang, C., Konopelko, A., & Cui, W. 2008, *ApJ*, 682, 1177
 Chevalier, R. A. 2000, *ApJ*, 539, L45
 Davies, B., Figer, D. F., Law, C. J., Kudritzki, R.-P., Najarro, F., Herrero, A., & MacKenty, J. W. 2008, *ApJ*, 676, 1016
 Djannati-Ataï, A., de Jager, O. C., Terrier, R., Gallant, Y. A., Hoppe, S. 2007, in *Proceedings of the 30th ICRC (Merida, Mexico)*, in press, (astro-ph/0710.2247)
 Dodson, R., Legge, D., Reynolds, J. E., & McCulloch, P. M. 2003, *ApJ*, 596, 1137
 Funk, S. 2007, *Ap&SS*, 309, 11
 Funk, S., Hinton, J. A., Pühlhofer, G., Aharonian, F. A., Hofmann, W., Reimer, O., & Wagner, S. 2007, *ApJ*, 662, 517
 Gaensler, B. M., Brazier, K. T. S., Manchester, R. N., Johnston, S., & Green, A. J. 1999, *MNRAS*, 305, 724
 Gaensler, B. M., Arons, J., Kaspi, V. M., Pivovarov, M. J., Kawai, N., & Tamura, K. 2002, *ApJ*, 569, 87
 Gaensler, B. M., Schulz, N. S., Kaspi, V. M., Pivovarov, M. J., & Becker, W. E. 2003, *ApJ*, 588, 441
 Gaensler, B. M., & Slane, P. O. 2006, *ARA&A*, 44, 17
 Gallant, Y. A. 2007, *Ap&SS*, 309, 197
 Ginzburg, V. L., & Syrovatskii, S. I. 1964, *The Origin of Cosmic Rays* (New York: Macmillan)
 Gotthelf, E. V., & Halpern, J. P. 2008, *ApJ*, 681, 515
 Helfand, D. J., Collins, B. F., & Gotthelf, E. V. 2003, *ApJ*, 582, 783
 Helfand, D. J., Gotthelf, E. V., Halpern, J. P., Camilo, F., Semler, D. R., Becker, R. H., & White, R. L. 2007, *ApJ*, 665, 1297
 Hinton, J. A. 2004, *NewA Rev.*, 48, 331
 Hinton, J. A., Funk, S., Carrigan, S., Gallant, Y. A., de Jager, O. C., Kosack, K., Lemièrre, A., Pühlhofer, G. 2007, *A&A*, 476, L25
 Kargaltsev, O., Pavlov, G. G., & Garmire, G. P. 2007, *ApJ*, 660, 1413
 Kargaltsev, O., & Pavlov, G. G. 2007, *ApJ*, 670, 655
 Kargaltsev, O., & Pavlov, G. G. 2008, in *AIP Conf. Proc.* 983, 171
 Kargaltsev, O., Pavlov, G. G., & Wong, J. A. 2008, *ApJ*, submitted (astro-ph/0805.1041)
 Kennel, C. F., & Coroniti, F. V. 1984a, *ApJ*, 283, 694
 Kennel, C. F., & Coroniti, F. V. 1984b, *ApJ*, 283, 710
 de Jager, O. C. and Djannati-Ataï, A. 2008, (astro-ph/0803.0116)
 Leahy, D. A., & Tian, W. W. 2008, *A&A*, 480, L25
 Livingstone, M. A., Kaspi, V. M., Gavriil, F. P., Manchester, R. N., Gotthelf, E. V. G., & Kuiper, L. 2007, *Ap&SS*, 308, 317
 Manchester, R. N. and Hobbs, G. B. and Teoh, A. and Hobbs, M. 2005, *AJ*, 129, 1993
 Manolakou, K., Horns, D. & Kirk, J. G. 2007, *A&A*, 474, 689
 Manzali, A., De Luca, A., & Caraveo, P. A. 2007, *ApJ*, 669, 570
 Ng, C.-Y., Roberts, M. S. E., & Romani, R. W. 2005, *ApJ*, 627, 904
 Porquet, D., Decourchelle, A., & Warwick, R. S. 2003, *A&A*, 401, 197
 Pacini, F., & Salvati, M. 1973, *ApJ*, 186, 249
 Possenti, A., Cerutti, R., Colpi, M., & Mereghetti, S. 2002, *A&A*, 387, 993
 Romani, R. W., Ng, C.-Y., Dodson, R., & Brisken, W. 2005, *ApJ*, 631, 480
 Rybicki, G. B., & Lightman, A. P. 1979, *Radiative Processes in Astrophysics* (New York: Wiley)
 Seward, F. D., & Wang, Z.-R. 1988, *ApJ*, 332, 199
 Slane, P., Chen, Y., Schulz, N. S., Seward, F. D., Hughes, J. P., & Gaensler, B. M. 2000, *ApJ*, 533, L29
 Slane, P., Helfand, D. J., Reynolds, S. P., Gaensler, B. M., Lemièrre, A., & Wang, Z. 2008, *ApJ*, 676, L33
 Trimble, V. 1973, *PASP*, 85, 579
 Willingale, R., Aschenbach, B., Griffiths, R. G., Sembay, S., Warwick, R. S., Becker, W., Abbey, A. F., & Bonnet-Bidaud, J.-M. 2001, *A&A*, 365, L212